


Article

# A DFT Calculation of Fluoride-Doped TiO<sub>2</sub> Nanotubes for Detecting SF<sub>6</sub> Decomposition Components

Xiaoxing Zhang <sup>1,2,\*</sup> , Jun Zhang <sup>1</sup>, Xingchen Dong <sup>1</sup> and Hao Cui <sup>1</sup>

<sup>1</sup> State Key Laboratory of Power Transmission Equipment & System Security and New Technology, Chongqing University, Chongqing 400044, China; junz2016@cqu.edu.cn (J.Z.); dxc\_cqu@outlook.com (X.D.); cuihaocqu@163.com (H.C.)

<sup>2</sup> School of Electrical Engineering, Wuhan University, Wuhan 430072, China

\* Correspondence: xiaoxing.zhang@outlook.com; Tel.: +86-136-2727-5072

Received: 21 July 2017; Accepted: 16 August 2017; Published: 18 August 2017

**Abstract:** Gas insulated switchgear (GIS) plays an important role in the transmission and distribution of electric energy. Detecting and analyzing the decomposed components of SF<sub>6</sub> is one of the important methods to realize the on-line monitoring of GIS equipment. In this paper, considering the performance limits of intrinsic TiO<sub>2</sub> nanotube gas sensor, the adsorption process of H<sub>2</sub>S, SO<sub>2</sub>, SOF<sub>2</sub> and SO<sub>2</sub>F<sub>2</sub> on fluoride-doped TiO<sub>2</sub> crystal plane was simulated by the first-principle method. The adsorption mechanism of these SF<sub>6</sub> decomposition components on fluorine-doped TiO<sub>2</sub> crystal plane was analyzed from a micro perspective. Calculation results indicate that the order of adsorption effect of four SF<sub>6</sub> decomposition components on fluoride-doped TiO<sub>2</sub> crystal plane is H<sub>2</sub>S > SO<sub>2</sub> > SOF<sub>2</sub> > SO<sub>2</sub>F<sub>2</sub>. Compared with the adsorption results of intrinsic anatase TiO<sub>2</sub> (101) perfect crystal plane, fluorine doping can obviously enhance the adsorption ability of TiO<sub>2</sub> (101) crystal plane. Fluorine-doped TiO<sub>2</sub> can effectively distinguish and detect the SF<sub>6</sub> decomposition components based on theoretical analysis.

**Keywords:** SF<sub>6</sub> decomposition component; fluorine-doped TiO<sub>2</sub>; first-principle simulation

## 1. Introduction

Gas insulated switchgear (GIS), with benefits such as small land cover, flexible configuration, high safety, and high reliability, has been widely used in the power system [1]. However, during the long-term operation of GIS equipment, the internal insulation defects may cause partial discharge (PD). SF<sub>6</sub> insulating gas in the GIS will decompose into some types of gases like SO<sub>2</sub>, H<sub>2</sub>S, SOF<sub>2</sub>, SO<sub>2</sub>F<sub>2</sub> [2–5] under the effect of PD. With the decomposition of SF<sub>6</sub>, aging of GIS equipment and corrosion of metal surface will be accelerated, which ultimately may lead to breakdown of GIS equipment, affecting the stable operation of the power system [6]. Therefore, it is of great importance to detect the SF<sub>6</sub> decomposition components in GIS equipment. On one hand, the type of PD can be confirmed by the types of decomposition components; on the other hand, by measuring the contents of decomposition, the level of PD can be determined, even the aging degree of GIS equipment. Therefore, through the monitoring of decomposition components, unnecessary losses can be reduced by timely taking precaution and preventing the breakdown of GIS equipment.

At present, utilizing the gas sensor method to achieve the goal of detecting SF<sub>6</sub> decomposition components has advantages of a small detection unit, easy installation process, fast detection speed, and so on. Therefore, it is of great importance to study gas sensitive response of the gas sensors made of different gas-sensing materials. Our team studied the gas-sensing materials such as carbon nanotubes and graphene [7–12]. However, it is in the early stage of research, and further research

needs to be conducted. At the same time, with the technology of TiO<sub>2</sub> nanotube preparation becoming mature, the TiO<sub>2</sub> nanotube gas sensor has advantages of high specific surface area and high symmetry, which makes it a research hotspot in the gas detection field. However, the inherent energy gap of TiO<sub>2</sub> is comparatively large (more than 3.0 eV), which hinders its wide development. Research shows that the surface of TiO<sub>2</sub> nanotubes can be modified by nonmetallic doping to improve its photosensitive, photocatalytic and other properties. Varghese et al [13,14] sputtered a layer of 10 nm thick of Pd on the surface of TiO<sub>2</sub> nanotubes by thermal evaporation, which can improve the sensitivity of TiO<sub>2</sub> nanotube gas sensor, and reduce the recovery time. More importantly, the improved sensor can detect H<sub>2</sub> at room temperature. At present, the study of nitrogen doping in nonmetallic doping has received the most attention [15–19]. The results show that nitrogen doping can reduce the energy gap of TiO<sub>2</sub>, which makes the electrons in the valence band transition more easily. In addition, many studies have reported that TiO<sub>2</sub> is modified by fluorine doping [20–23]. Fluorine doping does not basically change the size of the TiO<sub>2</sub> energy gap, but it can promote the generation of oxygen hole defects, increase the surface acidity and Ti<sup>3+</sup>, which is beneficial to reducing the recombination rate of electron hole pairs, and thereby improving the photocatalytic activity [24].

With the successful doping of fluorine onto the surface of TiO<sub>2</sub> [20,25,26], the study of application of fluorine-doped TiO<sub>2</sub> nanomaterials in gas sensing detection is deficient. In this paper, the idea of using fluorine-doped TiO<sub>2</sub> nanotubes gas sensor to detect SF<sub>6</sub> decomposition components was determined. The adsorption process of H<sub>2</sub>S, SO<sub>2</sub>, SOF<sub>2</sub> and SO<sub>2</sub>F<sub>2</sub> gas molecules onto fluorine-doped anatase TiO<sub>2</sub> (101) perfect crystal plane by first-principle calculation. The calculation parameters include adsorption energy, adsorption distance, charge transfer amount and the density of states. The simulation analysis can provide insight for the practical explanation of fluorine-doped TiO<sub>2</sub> nanometer array gas sensor detecting SF<sub>6</sub> decomposition gases from the microscopic point of view. Finally, the adsorption results of SO<sub>2</sub>, SOF<sub>2</sub> and SO<sub>2</sub>F<sub>2</sub> under different doping conditions were compared in this paper.

## 2. Calculation Parameters and Methods

The TiO<sub>2</sub> model in this paper is an anatase TiO<sub>2</sub> (101) perfect facet model derived directly from the database provided by Materials Studio software, and the size is 3.776 × 3.776 × 9.486 Å, which is the smallest unit of anatase TiO<sub>2</sub>. The detailed calculation process is as follows: build the anatase TiO<sub>2</sub> (101) perfect crystal plane 2 × 2 super-cell model, and the gas molecules of SO<sub>2</sub>, H<sub>2</sub>S, SOF<sub>2</sub> and SO<sub>2</sub>F<sub>2</sub>; optimize these models initially in the Dmol<sup>3</sup> module, which can make these micro-structure parameters to maximumly close to the idealization, as shown in Figure 1.; replace one of the O atoms on the surface of the anatase TiO<sub>2</sub> (101) perfect crystal plane by F atom; After optimized treatment, the fluorine doped anatase TiO<sub>2</sub> (101) perfect crystal plane supercell model (F-doped TiO<sub>2</sub>) is obtained, as shown in Figure 2; finally, the optimized SO<sub>2</sub>, H<sub>2</sub>S, SOF<sub>2</sub> and SO<sub>2</sub>F<sub>2</sub> gas molecules with different postures approach respectively close to the surface of the perfect crystal plane of the anatase TiO<sub>2</sub> (101) to get a different adsorption system. Different adsorption systems were optimized in order to find a more stable adsorption structure for each gas molecule onto F-doped TiO<sub>2</sub>.

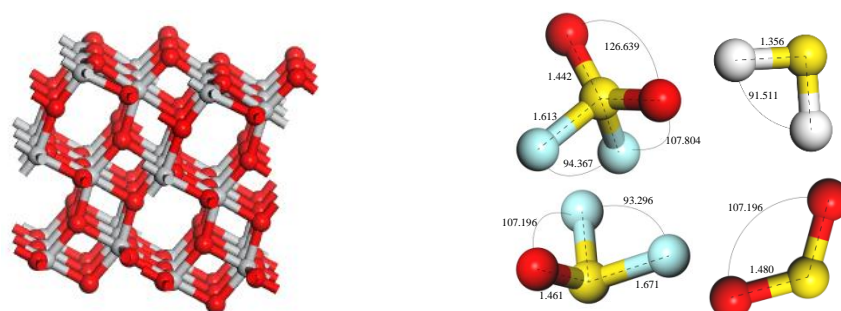


**Figure 1.** Perfect crystal model of intrinsic anatase TiO<sub>2</sub> (101) and SO<sub>2</sub>, H<sub>2</sub>S, SOF<sub>2</sub> and SO<sub>2</sub>F<sub>2</sub> gas molecular models, Ti atom is grey, O atom is red, S atom is yellow, F atom is blue, H atom is white.

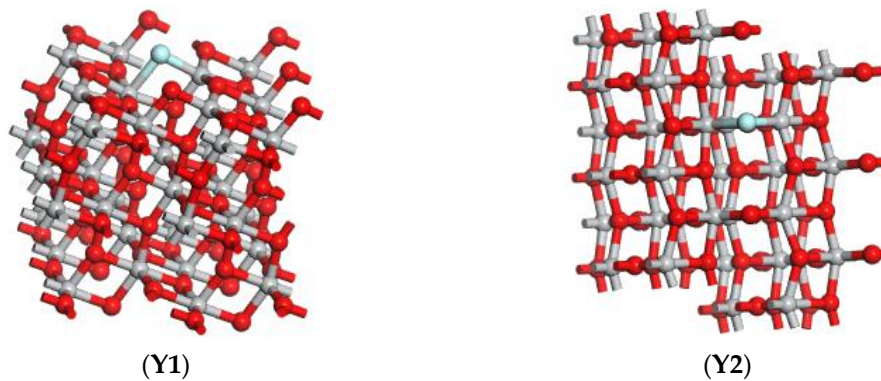


**Figure 2.** F-doped TiO<sub>2</sub> model, (Y1) is the main view of the model, and (Y2) is the top view of the model.

In this paper, parameters are set as follows when optimizing the calculation. Since the number of atoms contained in the perfect crystal plane model of the anatase TiO<sub>2</sub> (101) established in this paper is large, the generalized gradient approximate (GGA) with high calculation accuracy was adopted so as to make the calculated physical and chemical characteristics of the different adsorption system more accurate. The exchange and correlation interaction effect between electrons were represented by the Perdew-Burke-Ernzerhof (PBE) function [27]. The energy convergence tolerance and the energy gradient (max. force) are set to  $1.0 \times 10^{-5}$  Ha and 0.002 Ha/Å respectively. The atomic displacement (max. displacement) is set to 0.005 Å. The convergence accuracy of the self-consistent field charge density (SCF tolerance) is set to  $1.0 \times 10^{-6}$  Ha, Brillouin k-point grid (k-point) is set to  $2 \times 2 \times 1$ ; the double Numeric Basis with Polarization (DNP) was used in the atomic orbits calculation with d, p orbital polarization function at the same time so as to make the results more accurate. Considering the influence of the dispersion force, that is, the van der Waals force, the DFT-D (Grimme) algorithm was utilized; in order to improve the efficiency of computation, the direct inversion of iterative subspace (DIIS) is used to improve the convergence rate of the charge density of the self-consistent field.

### 3. Simulation Results and Analysis

#### 3.1. Establishment of F-Doped TiO<sub>2</sub> Model

The F-doped TiO<sub>2</sub> model was established based on the perfect crystal plane model. A fluorine atom replaces one of the O atoms on the surface of the anatase TiO<sub>2</sub> (101) perfect crystal plane, and F atom combined with Ti atoms to form Ti-F bonds.

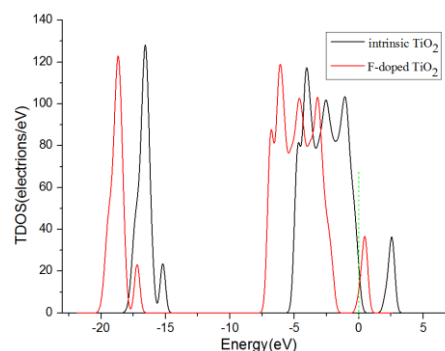


**Figure 3.** The curves of the density of states of F-doped TiO<sub>2</sub> and intrinsic anatase TiO<sub>2</sub> (101) perfect crystal plane, the green short dashed line is Fermi level.

Figure 3 shows the curve of the density of states (DOS) of F-doped TiO<sub>2</sub> and intrinsic anatase TiO<sub>2</sub> (101) perfect crystal plane. It can be seen from the figure that the peak and shape of the density

curve almost did not change after the fluorine atom being doped. The doping of the fluorine atoms hardly changes the band gap of  $\text{TiO}_2$ . However, after fluorine element doping, the  $\text{Ti}^{4+}$  is converted to  $\text{Ti}^{3+}$ , and the presence of a certain amount of  $\text{Ti}^{3+}$  will reduce the recombination rate of electron hole pairs [28]. Furthermore, fluorine element doping is conducive to the generation of oxygen holes and enhances the mobility of effective electrons [24,29], which can enhance the conductivity of the adsorbent substrate and improve the gas sensing performance of the fluorine-doped  $\text{TiO}_2$  nano array gas sensor mentioned above.

### 3.2. Parameter Calculation of Different Adsorption Systems

Figure 4 shows the adsorption structure of four gas molecules adsorbed on the F atom of the F-doped  $\text{TiO}_2$  crystal planes in different ways after complete optimization calculation. Due to the structural characteristics of four gas molecules, the way that the gas molecule adsorbed on the crystal plane was considered. Three situations are considered when the  $\text{SO}_2$  molecule comes close to the crystal plane in the optimization calculations, that is a single S and O atoms close to the crystal plane and two O atoms simultaneously close to the crystal plane. And the adsorption structures after calculation are shown in Figure 4a–c. Three cases were considered for  $\text{H}_2\text{S}$  molecules: the single S, H atoms close to the crystal plane and two H atoms simultaneously close to the crystal plane. The calculated adsorption structures are shown in Figure 4d–f.  $\text{SOF}_2$  molecules mainly consider four cases: the single S, O, F atoms close to the crystal plane and two F atoms simultaneously close to the crystal plane, the calculated adsorption structure are shown in Figure 4g–j; the  $\text{SO}_2\text{F}_2$  molecule is of a tetrahedral structure, and the S atom is inside the structure. So,  $\text{SO}_2\text{F}_2$  mainly considers 4 cases: a single O, F atom close to the crystal plane, two O atoms and two F atoms are simultaneously close to the crystal plane, separately. The calculated adsorption structures are shown in Figure 4k–n.

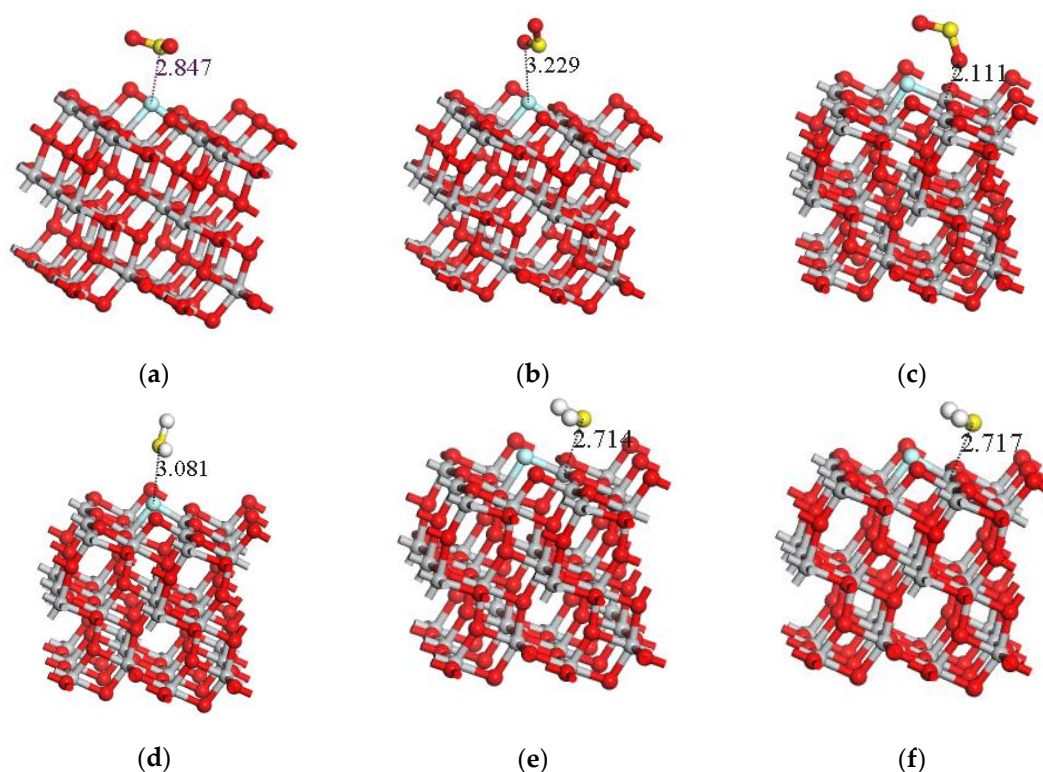
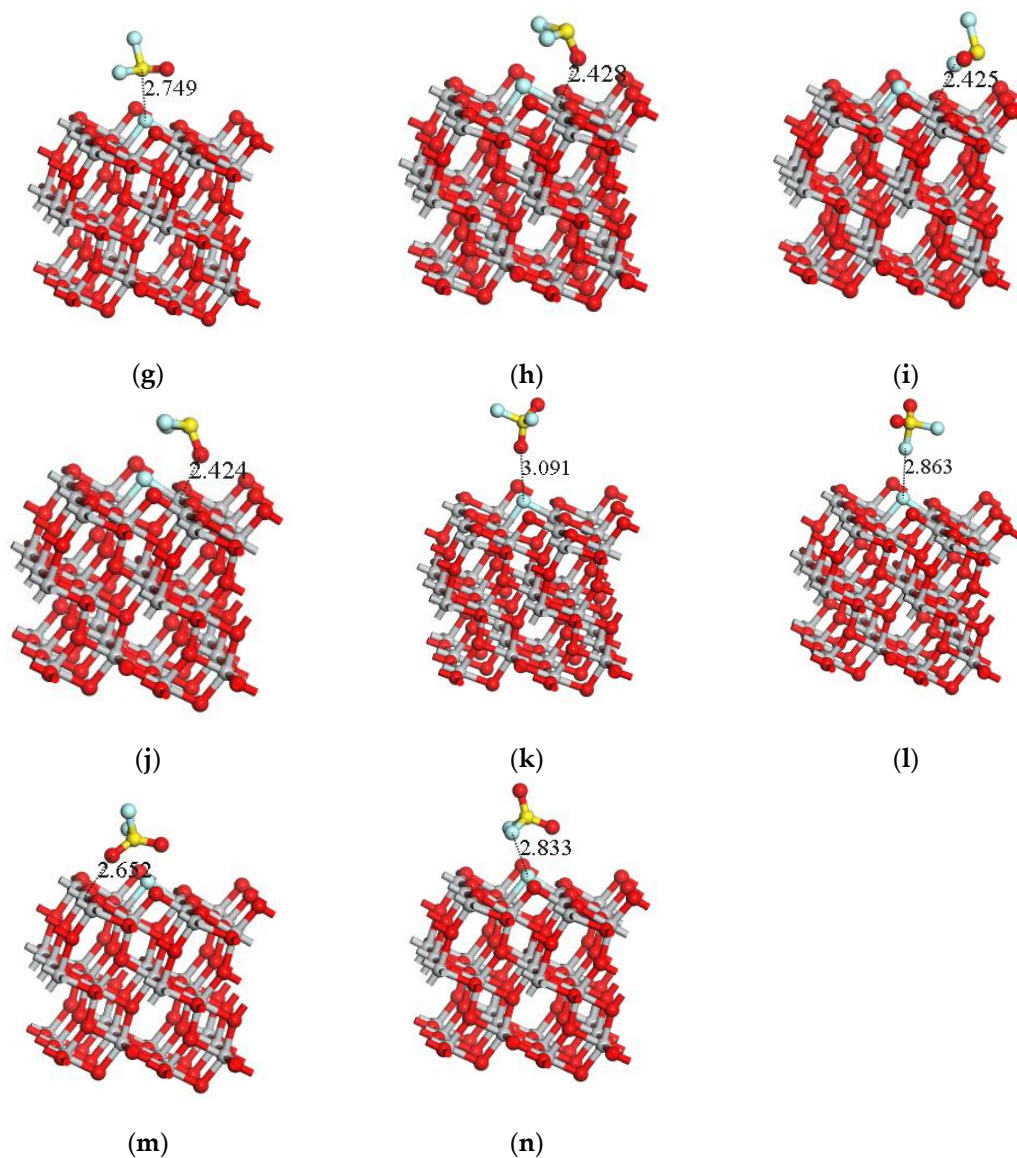


Figure 4. Cont.



**Figure 4.** The adsorption structures of four gas molecules adsorbed on the crystal surface in different ways. (a–n) are the adsorption structure of four gas molecules adsorbed on the F-doped TiO<sub>2</sub> crystal plane in different ways after complete optimization calculation.

Adsorption energy is the degree of change of total energy before and after the adsorption of gas molecules onto crystal plane, which represents the ability of gas molecules adsorption onto the crystal plane. In this paper, the magnitude of adsorption energy is expressed by  $E_a$ , and the formula is as follows:

$$E_a = E_{\text{sys}} - E_{\text{gas}} - E_{\text{sur}}, \quad (1)$$

where  $E_{\text{sys}}$  represents the energy of the whole system after the gas adsorbed on the F-doped TiO<sub>2</sub>,  $E_{\text{gas}}$  represents the energy when the gas molecules are present alone, and  $E_{\text{sur}}$  represents the energy of F-doped TiO<sub>2</sub> without the adsorption of gas molecules.

In the adsorption process, besides the change of energy, it may also be accompanied with the electron transfer, which results in the change of the electronic structure of the crystal plane, and shows the changes of electrical properties such as resistance and capacitance at macro level. In practical applications, the gas sensitive response characteristics of gas sensors can be obtained by detecting these electrical characteristics. Therefore, this paper also calculated Mulliken charge distribution of

the gas molecules adsorbed onto the F-doped TiO<sub>2</sub>, to confirm the amount of charge transfer before and after the adsorption of gas molecules onto the crystal plane. The charge transfer  $Q_t$  is defined as the charge change of gas molecules before and after they are adsorbed onto the F-doped TiO<sub>2</sub> crystal plane. If  $Q_t > 0$ , the electron is transferred from the gas molecule to the crystal plane. On the contrary, if  $Q_t < 0$ , part of the electrons is transferred from the crystal plane to the gas molecule. Table 1 shows the adsorption energies, adsorption distance and charge transfer of four kinds of gas molecules SO<sub>2</sub>, H<sub>2</sub>S, SOF<sub>2</sub> and SO<sub>2</sub>F<sub>2</sub> adsorbed onto F-doped TiO<sub>2</sub> crystal plane in different postures.

**Table 1.** Adsorption parameters of four gas molecules on the perfect crystal plane of F-doped TiO<sub>2</sub>.

Adsorption System	Adsorption Structure	Adsorption Energy $E_a$ (eV)	Charge transfer Amount $Q_t$ (e)	Adsorption Distance (Å)
SO <sub>2</sub> -S-TiO <sub>2</sub>	a	−0.173	−0.013	2.847
SO <sub>2</sub> -O-TiO <sub>2</sub>	b	−0.132	0	3.229
SO <sub>2</sub> -2O-TiO <sub>2</sub>	c	−0.617	−0.12	2.111
H <sub>2</sub> S-S-TiO <sub>2</sub>	d	−0.209	0.008	2.835
H <sub>2</sub> S-H-TiO <sub>2</sub>	e	−0.837	0.267	2.714
H <sub>2</sub> S-2H-TiO <sub>2</sub>	f	−0.836	0.266	2.717
SOF <sub>2</sub> -S-TiO <sub>2</sub>	g	−0.254	−0.017	2.749
SOF <sub>2</sub> -O-TiO <sub>2</sub>	h	−0.412	0.098	2.438
SOF <sub>2</sub> -F-TiO <sub>2</sub>	i	−0.534	0.038	2.425
SOF <sub>2</sub> -2F-TiO <sub>2</sub>	j	−0.423	0.098	2.424
SO <sub>2</sub> F <sub>2</sub> -O-TiO <sub>2</sub>	k	−0.044	0	3.091
SO <sub>2</sub> F <sub>2</sub> -F-TiO <sub>2</sub>	l	−0.051	−0.002	2.863
SO <sub>2</sub> F <sub>2</sub> -2O-TiO <sub>2</sub>	m	−0.398	0.046	2.652
SO <sub>2</sub> F <sub>2</sub> -2F-TiO <sub>2</sub>	n	−0.198	−0.003	2.833

In Table 1, SO<sub>2</sub>-S-TiO<sub>2</sub> represents an adsorption system in which SO<sub>2</sub> molecules are close to the F-doped TiO<sub>2</sub> crystal plane with single S atom, and others are similar.  $E_a < 0$  indicates that the adsorption of four kinds of molecules onto F-doped TiO<sub>2</sub> crystal plane are exothermic. The value of  $E_a$  is larger, indicates that the adsorption of gas molecules onto F-doped TiO<sub>2</sub> crystal plane is easier, and adsorption structure is more stable.

When H<sub>2</sub>S gas molecules with a single H atom close to the crystal plane and two H atoms simultaneously close to crystal plane, the adsorption structure after optimization calculation (Figure 4e,f) is almost the same, the calculated adsorption energy (−0.837 eV and −0.836 eV) and the amount of charge transfer (0.267 e and 0.266 e) is almost exactly the same, which is larger than the adsorption energy and charge transfer (−0.209 eV and 0.008 e) of the adsorption with single S atom close to the crystal plane. At the same time, the adsorption distance (2.835 Å) of the adsorption system obtained from H<sub>2</sub>S gas molecules with single S atom close to the crystal plane should be larger than that of the other two approaching ways (2.714 Å and 2.717 Å). Therefore, the H<sub>2</sub>S gas molecules are much easier to adsorb onto the crystal plane with a single H atom close to the crystal plane and two H atoms simultaneously close to the F-doped TiO<sub>2</sub> crystal plane. When the H<sub>2</sub>S gas molecules are adsorbed on the crystal plane, the amount of charge transferred to the crystal plane is about 0.266 e, and the macroscopic gas sensitivity of the gas sensor shows the decrease of the impedance.

Similarly, the adsorption reaction of SOF<sub>2</sub> gas molecules more easily occurs in three cases: close to the F-doped TiO<sub>2</sub> surface with a single O and F atoms and two F atoms at the same time, and the macroscopic sensitivity of the gas sensor shows the decrease of the impedance. SO<sub>2</sub> gas molecule reacts easier with two O atoms at the same time when approaching the crystal surface, and the macroscopic gas sensitivity of the gas sensor shows the increase of the impedance. The comparison shows that the adsorption energy of H<sub>2</sub>S gas molecules onto F-doped TiO<sub>2</sub> crystal plane is the highest, which is about two times of that of SOF<sub>2</sub>, SO<sub>2</sub>F<sub>2</sub>. In addition, when the three types of gas molecules, H<sub>2</sub>S, SOF<sub>2</sub> and SO<sub>2</sub>F<sub>2</sub>, adsorb onto F-doped TiO<sub>2</sub>, the macroscopic gas sensitivity of the gas sensor shows the decrease of the impedance. When SO<sub>2</sub> gas molecules react onto the F-doped TiO<sub>2</sub>, the macroscopic gas

sensitivity of the gas sensor shows the increase of the impedance. Therefore, theoretically, F-doped  $\text{TiO}_2$  nanotube array gas sensor can effectively distinguish and detect the four kinds of gases.

### 3.3. Analysis of Density of States

When different gas molecules adsorb on the surface of the gas sensor, the resistance of the sensor may change; the fluorine-doped  $\text{TiO}_2$  nanotube array gas sensor mainly uses this principle to achieve the detection of  $\text{SF}_6$  decomposition components. So, one of the key parameters in practical applications is the resistance of the sensor and analysis of DOS of the adsorption system can be used to find the reasons from the change in resistance.

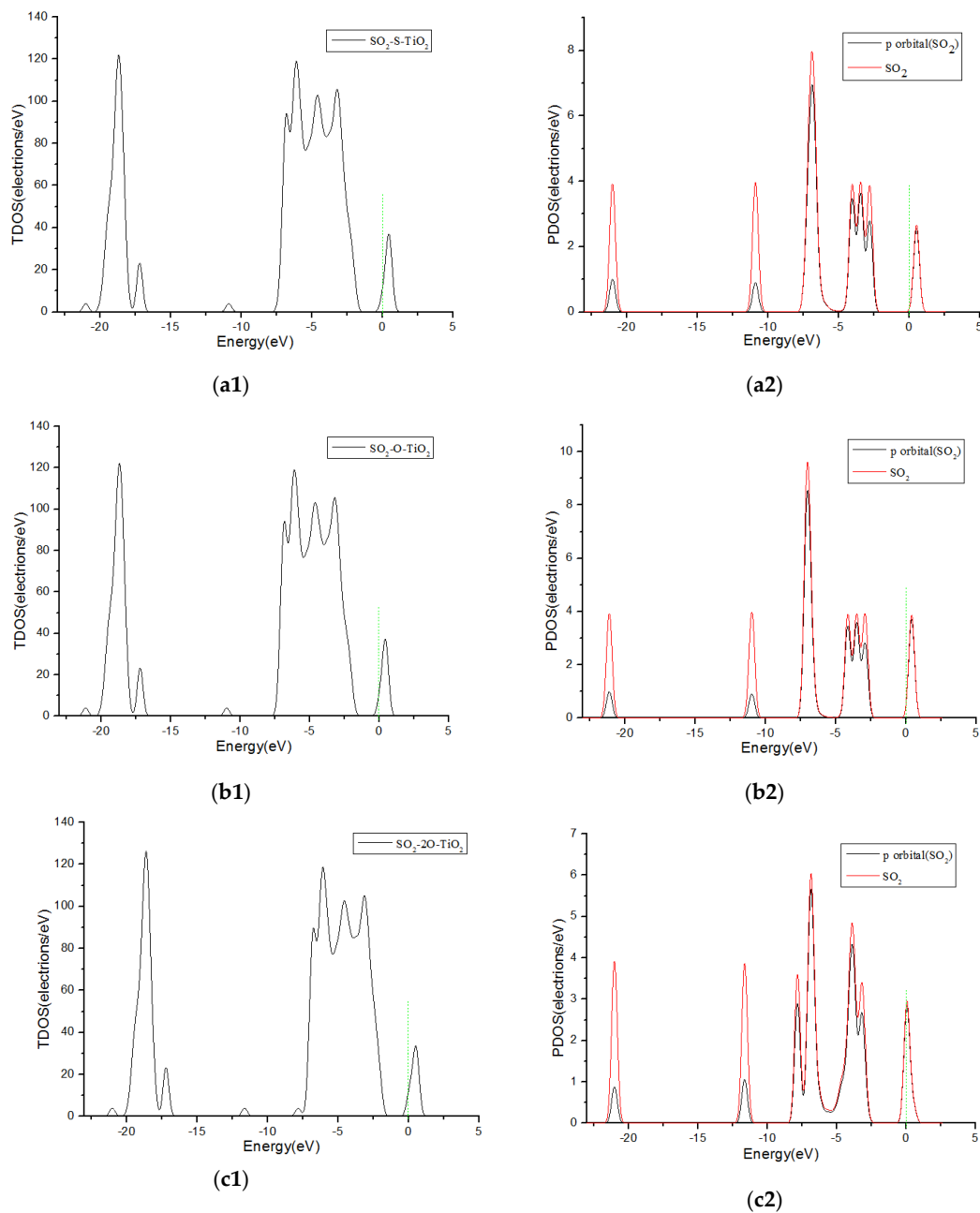


**Figure 5.** The total density and partial density of  $\text{SO}_2$  molecules adsorbed on F-doped  $\text{TiO}_2$ , and the green short dashed line is Fermi level. (a1,a2) are the TDOS and PDOS of  $\text{SO}_2$ -S- $\text{TiO}_2$ , (b1,b2) are the TDOS and PDOS of  $\text{SO}_2$ -O- $\text{TiO}_2$ , (c1,c2) are the TDOS and PDOS of  $\text{SO}_2$ -2O- $\text{TiO}_2$ .

Figure 5 shows the total density of states (TDOS) and the partial density of states (PDOS) curves of  $\text{SO}_2$  molecules adsorbed on F-doped  $\text{TiO}_2$ . Since the contributes of p-orbit of the gas molecule is greatest to DOS, it is also presented in the figure. It can be seen from Figure 5(a1–b2), when the single S atom and the single O atom are close to the F-doped  $\text{TiO}_2$  crystal plane, the  $\text{SO}_2$  gas molecules contribute to the DOS of the adsorption system only on the right side of 0 eV. But, It can be seen from Figure 5(c1,c2), when the  $\text{SO}_2$  molecule close to the crystal plane with two O atoms at the same time, the  $\text{SO}_2$  molecules have a significant contribution to the DOS of the adsorption system on the both sides of 0 eV. This corresponds to the charge transfer amount ( $-0.013$  e,  $0$  e and  $-0.12$  e, respectively) when the  $\text{SO}_2$  molecules are adsorbed in three different ways in Table 1. It is shown that  $\text{SO}_2$  molecules are more likely to react and adsorb on the crystal plane approaching in the form of with two O atoms. The theoretical analysis shows that  $\text{SO}_2$  gas obtain electrons when adsorbed onto the fluorine-doped  $\text{TiO}_2$  nano sensors, and the macroscopic gas-sensing properties show an increase in impedance.

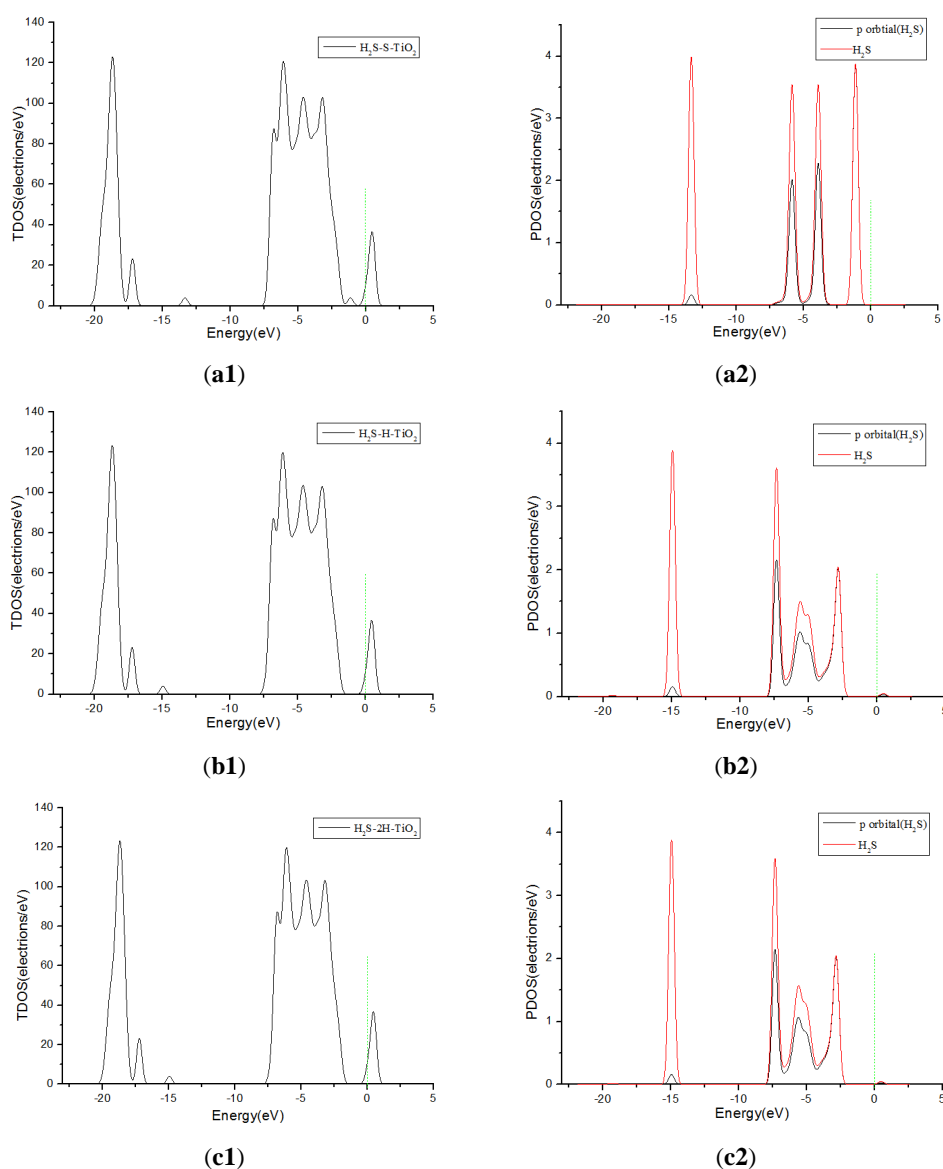


**Figure 6.** TDOS and PDOS of  $\text{H}_2\text{S}$  molecules adsorbed onto F-doped  $\text{TiO}_2$ , and the green short dashed line is Fermi level. (a1,a2) are the TDOS and PDOS of  $\text{H}_2\text{S-S-TiO}_2$ , (b1,b2) are the TDOS and PDOS of  $\text{H}_2\text{S-H-TiO}_2$ , (c1,c2) are the TDOS and PDOS of  $\text{H}_2\text{S-2H-TiO}_2$ .



Figure 6 shows TDOS and PDOS curves of H<sub>2</sub>S molecules adsorbed onto F-doped TiO<sub>2</sub>. When the H<sub>2</sub>S gas molecules close to the F-doped TiO<sub>2</sub> crystal plane with single S atom, the gas molecules have little contribution to DOS at 0 eV in Figure 6(a1,a2). However, when H<sub>2</sub>S molecules approach the F-doped TiO<sub>2</sub> crystal plane with single H atom and two H atoms at the same time separately, the molecules have a significant contribution to the DOS on the right side of 0 eV in Figure 6(b1–c2). This corresponds to the charge transfer amount (0.008 e, 0.267 e and 0.266 e, respectively) when the H<sub>2</sub>S molecule close to the crystal plane with single S atom, single H atom and two H atoms at the same time in Table 1. It is shown that H<sub>2</sub>S molecules are more likely to be adsorbed on the crystal plane approaching in the form of a single H atom and two H atoms at the same time. Similarly, SOF<sub>2</sub> gas molecules are more likely to adsorb by single O, single F atom, and two F atoms at the same time when coming close to the crystal plane than by single S atom. The TDOS and PDOS curves of SOF<sub>2</sub> adsorption systems are shown in Figure 7. The theoretical analysis shows that H<sub>2</sub>S and SOF<sub>2</sub> gases lose electrons when adsorbed onto the fluorine-doped TiO<sub>2</sub> nano sensors, and the macroscopic gas-sensing properties show a decrease in impedance. Furthermore, the changed value of impedance of H<sub>2</sub>S is bigger than SOF<sub>2</sub>.

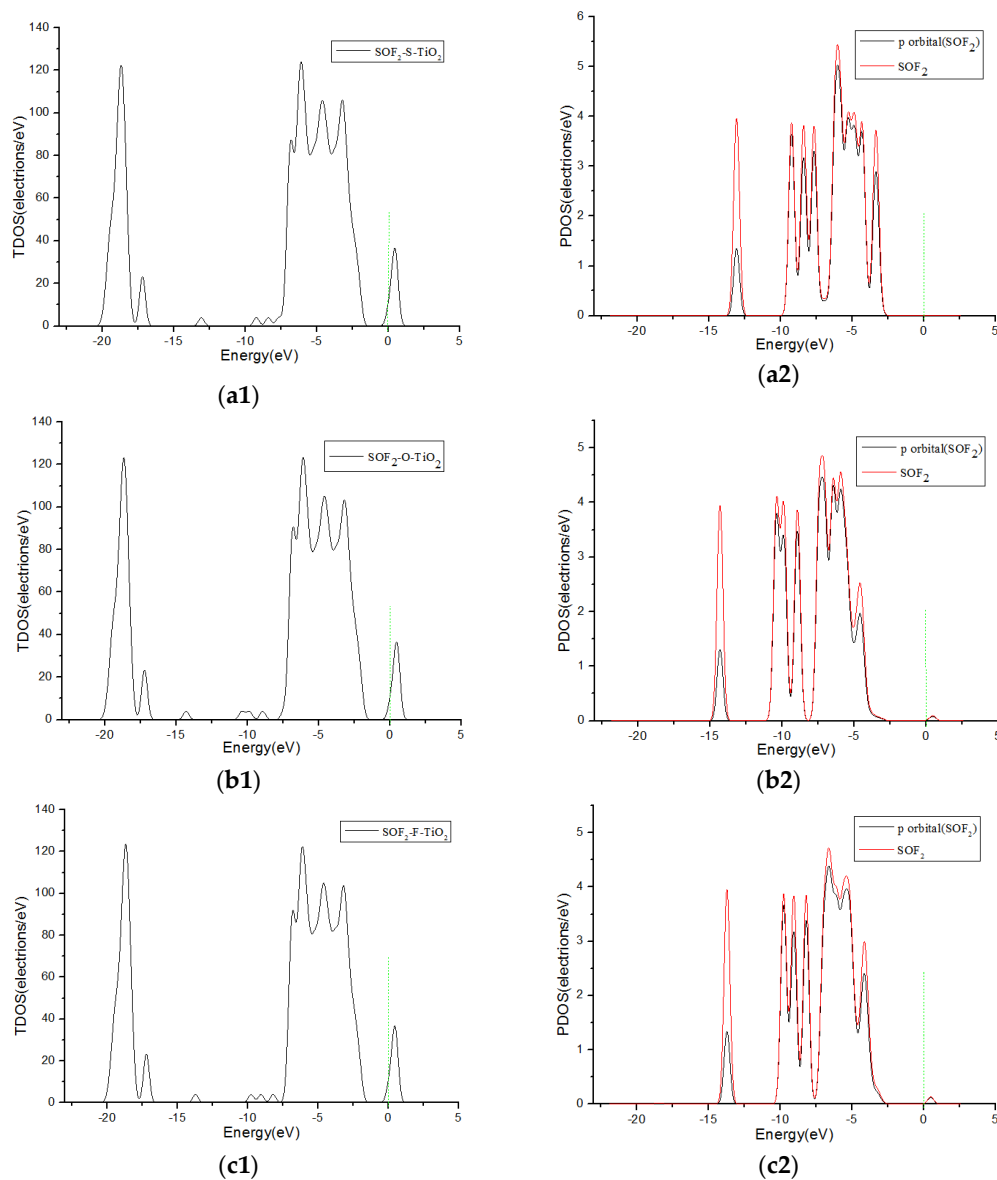
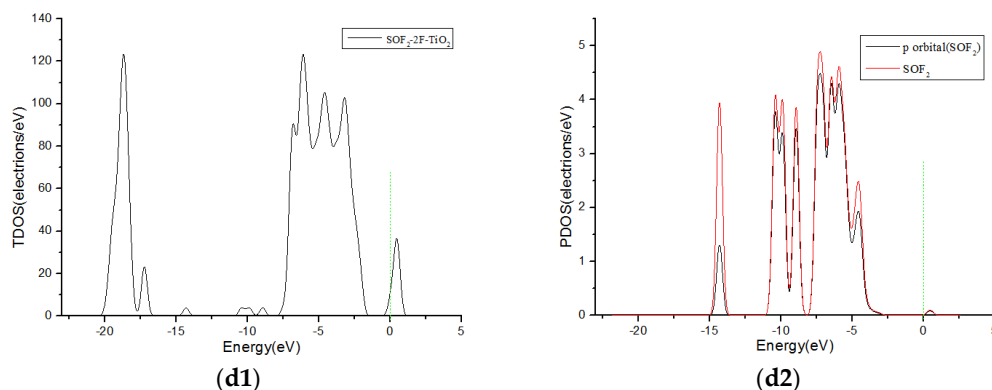
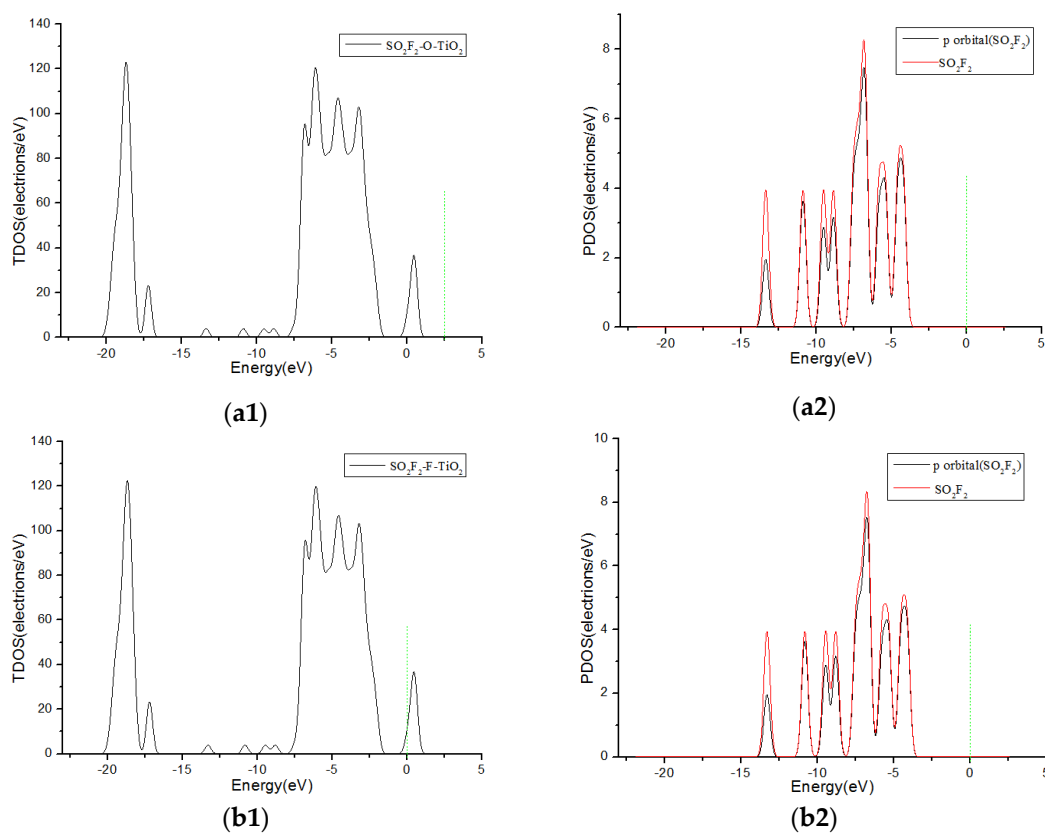


Figure 7. Cont.



**Figure 7.** TDOS and PDOS of  $\text{SOF}_2$  molecules adsorbed onto F-doped  $\text{TiO}_2$ , and the green short dashed line is Fermi level. (a1,a2) are the TDOS and PDOS of  $\text{SOF}_2$ -S- $\text{TiO}_2$ , (b1,b2) are the TDOS and PDOS of  $\text{SOF}_2$ -O- $\text{TiO}_2$ , (c1,c2) are the TDOS and PDOS of  $\text{SOF}_2$ -F- $\text{TiO}_2$ , (d1,d2) are the TDOS and PDOS of  $\text{SOF}_2$ -2F- $\text{TiO}_2$ .

No matter which way the  $\text{SO}_2\text{F}_2$  gas molecules approaching the crystal surface, the contribution to the DOS is almost 0 on both sides of 0eV, as shown in Figure 8. It can also be seen from Table 1 that the charge transfer is very small when  $\text{SO}_2\text{F}_2$  molecules come close to the F-doped  $\text{TiO}_2$  crystal plane. The theoretical analysis indicates that the changed value of impedance of  $\text{SO}_2\text{F}_2$  is small on the macro level when adsorbed onto the fluorine-doped  $\text{TiO}_2$  nano sensors. It can be assumed that the selectivity of fluorine-doped  $\text{TiO}_2$  nanotubes gas sensor to  $\text{SO}_2\text{F}_2$  gas is weak.



**Figure 8.** Cont.

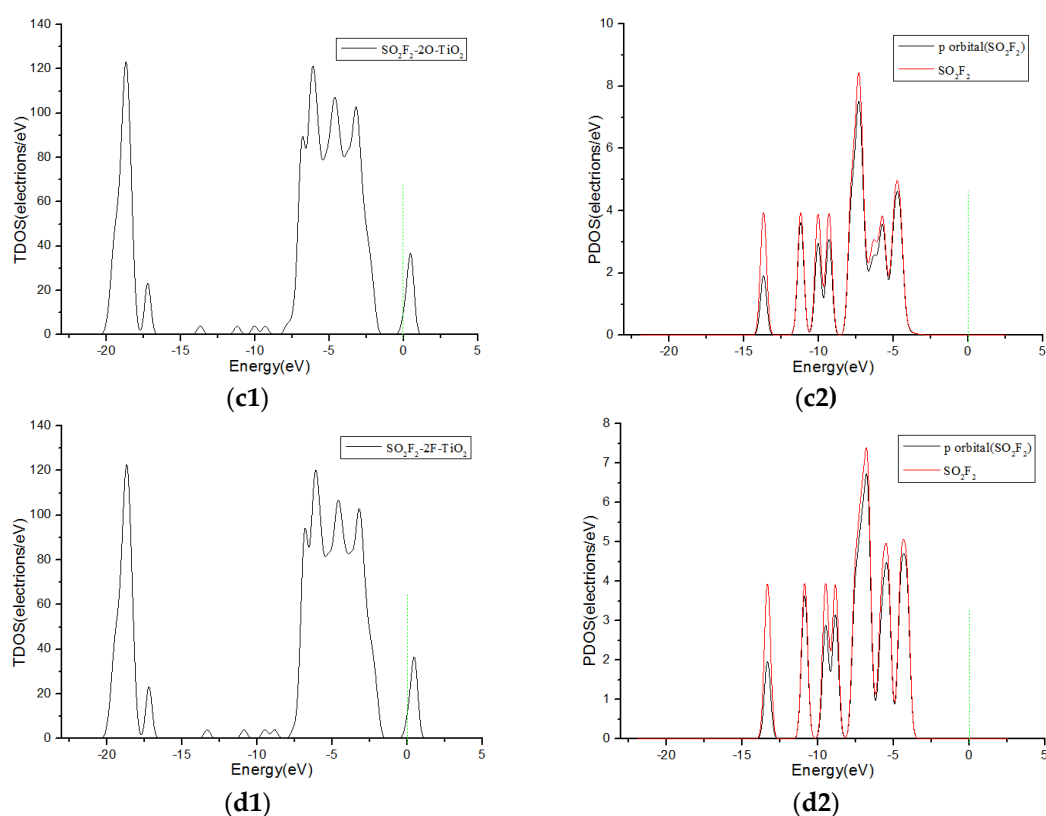


**Figure 8.** TDOS and PDOS of  $\text{SO}_2\text{F}_2$  molecules adsorbed on F-doped  $\text{TiO}_2$ , and the green short dashed line is Fermi level. (a1,a2) are the TDOS and PDOS of  $\text{SO}_2\text{F}_2\text{-O-TiO}_2$ , (b1,b2) are the TDOS and PDOS of  $\text{SO}_2\text{F}_2\text{-F-TiO}_2$ , (c1,c2) are the TDOS and PDOS of  $\text{SO}_2\text{F}_2\text{-2O-TiO}_2$ , (d1,d2) are the TDOS and PDOS of  $\text{SO}_2\text{F}_2\text{-2F-TiO}_2$ .

### 3.4. Comparison of Adsorption Results under Different Doping Conditions

The reference [30] shows the adsorption results of  $\text{SO}_2$ ,  $\text{SOF}_2$  and  $\text{SO}_2\text{F}_2$  onto the intrinsic anatase  $\text{TiO}_2$  (101) perfect crystal plane. By comparison, the adsorption structure of the three kinds of gas molecules adsorbed on the intrinsic anatase  $\text{TiO}_2$  (101) perfect crystal plane in the reference is similar to that of Figure 4c,h,m. Therefore, in order to make the comparison results more meaningful, adsorption parameters of adsorption structure in Figure 4c,h,m were chosen to be compared.

After fluorine doping on the anatase  $\text{TiO}_2$  (101) perfect crystal plane, the adsorption energy and charge transfer amount of the  $\text{SO}_2$ ,  $\text{SOF}_2$  and  $\text{SO}_2\text{F}_2$  gas molecules adsorption system obviously increased, and the adsorption distance also decreased correspondingly. In addition, the adsorption energy of  $\text{SO}_2$  gas molecules adsorbed on F-doped  $\text{TiO}_2$  crystal plane is  $-0.617$  eV, which indicates that the adsorption of  $\text{SO}_2$  gas molecules onto the F-doped  $\text{TiO}_2$  crystal plane was chemical adsorption.

The DOS were also compared and analyzed. In this paper, the corresponding TDOS and PDOS of the adsorption structures of three gas molecules are shown in Figure 5(c1,c2), Figure 7(b1,b2) and Figure 8(c1,c2). It was found that the contribution of  $\text{SO}_2$  and  $\text{SOF}_2$  molecules to the PDOS near 0eV significantly increased after fluorine doping, which corresponded to the charge transfer of the adsorption systems in the two cases. Because the crystal shows weak adsorption reaction to  $\text{SO}_2\text{F}_2$  gas molecules before and after doping, the contribution of  $\text{SO}_2\text{F}_2$  gas molecules to PDOS did not changed much at 0 eV. Through the above analysis, it can be concluded that the adsorption ability of the anatase  $\text{TiO}_2$  (101) crystal plane to the three gas molecules is enhanced after fluorine doping.

Reference [31] reported modified  $\text{TiO}_2$  crystal plane by nitrogen doping to detect  $\text{SF}_6$  decomposition components. It can be seen that  $\text{SO}_2$  molecules are more likely to adsorb on nitrogen-doped  $\text{TiO}_2$  crystal plane with S atom.  $\text{SOF}_2$  is more likely to adsorb on nitrogen-doped  $\text{TiO}_2$

crystal plane with O and S atoms, respectively. The adsorption of SO<sub>2</sub> and SOF<sub>2</sub> on nitrogen-doped TiO<sub>2</sub> crystal plane is stronger than that on fluorine-doped TiO<sub>2</sub> crystal plane. However, when nitrogen-doped TiO<sub>2</sub> crystal plane reacts with SO<sub>2</sub> and SOF<sub>2</sub>, the adsorption energy, charge transfer amount and adsorption distance have little difference, and the macro-gas-sensing characteristics all show the decrease of impedance. Therefore, nitrogen-doped TiO<sub>2</sub> cannot effectively distinguish SO<sub>2</sub> and SOF<sub>2</sub>. When fluorine-doped TiO<sub>2</sub> crystal plane react with SO<sub>2</sub>, SO<sub>2</sub> molecule obtains electrons, and fluorine-doped TiO<sub>2</sub> gas sensor macro-gas-sensing characteristics show the increase of impedance. When fluorine-doped TiO<sub>2</sub> crystal plane adsorb SOF<sub>2</sub>, SOF<sub>2</sub> molecule loses electrons, and fluorine-doped TiO<sub>2</sub> gas sensor macro-gas-sensing characteristics show the decrease of impedance. Although the adsorption of SO<sub>2</sub> and SOF<sub>2</sub> on fluorine-doped TiO<sub>2</sub> crystal plane is weaker than that of nitrogen-doped TiO<sub>2</sub> crystal plane, fluorine-doped TiO<sub>2</sub> can effectively distinguish SO<sub>2</sub> and SOF<sub>2</sub>.

#### 4. Conclusions

In this paper, one O atom of the anatase TiO<sub>2</sub> (101) perfect crystal plane is replaced by one F atom to obtain a fluorine-doped anatase TiO<sub>2</sub> (101) perfect crystal plane model. H<sub>2</sub>S, SO<sub>2</sub>, SOF<sub>2</sub> and SO<sub>2</sub>F<sub>2</sub> of SF<sub>6</sub> decomposition components adsorb on the F-doped TiO<sub>2</sub> crystal plane in different ways to obtain different adsorption systems, which were then optimized. The adsorption mechanism is obtained by the optimized adsorption parameters. The adsorption results were compared and analyzed with intrinsic and nitrogen doping, with the effects of different doping on adsorption parameters studied. Through the above analysis, the following conclusions are drawn:

(1) Four kinds of gas molecules are close to the crystal plane, which cause gas molecules to be adsorbed on the crystal plane more easily. The adsorption ability of four kinds of gas molecules onto F-doped TiO<sub>2</sub> crystal plane is: H<sub>2</sub>S > SO<sub>2</sub> > SOF<sub>2</sub> > SO<sub>2</sub>F<sub>2</sub>.

(2) The adsorption capacity of TiO<sub>2</sub> to SO<sub>2</sub>, SOF<sub>2</sub> and SO<sub>2</sub>F<sub>2</sub> is obviously enhanced after fluorine doping, and the degree of the adsorption to SO<sub>2</sub> gas molecules has reached the chemical adsorption.

(3) Based on the change of resistance of fluorine-doped TiO<sub>2</sub> sensors on the macro level can effectively distinguish SO<sub>2</sub> and SOF<sub>2</sub> from theoretical analysis, even though the adsorption of SF<sub>6</sub> decomposition components onto nitrogen-doped TiO<sub>2</sub> crystal plane is stronger than that on fluorine-doped TiO<sub>2</sub> crystal plane.

**Acknowledgments:** We gratefully acknowledge the financial support from National Natural Science Foundation of P.R. China (project No. 51277188).

**Author Contributions:** Xiaoxing Zhang designed the project, instructed the research and modified the manuscript. Jun Zhang wrote and modified the manuscript. Fan Liu, Xingchen Dong and Hao Cui modified the manuscript.

**Conflicts of Interest:** The authors declare no conflict of interest.

#### References

1. Zeng, F.; Tang, J.; Fan, Q.; Pan, J.; Zhang, X.; Yao, Q.; He, J. Decomposition characteristics of SF<sub>6</sub> under thermal fault for temperatures below 400 °C. *IEEE Trans. Dielectr. Electr. Insul.* **2014**, *21*, 995–1004. [[CrossRef](#)]
2. Dourdour, A.; Casanovas, J.; Hergli, R.; Grob, R.; Mathieu, J. Study of the decomposition of wet SF<sub>6</sub>, subjected to 50-Hz ac corona discharges. *J. Appl. Phys.* **1989**, *65*, 1852–1857. [[CrossRef](#)]
3. Tang, J.; Zeng, F.; Pan, J.; Zhang, X.; Yao, Q.; He, J.; Hou, X. Correlation analysis between formation process of SF<sub>6</sub> decomposed components and partial discharge qualities. *IEEE Trans. Dielectr. Electr. Insul.* **2013**, *20*, 864–875. [[CrossRef](#)]
4. Zeng, F.; Tang, J.; Zhang, X.; Xie, Y.; Yao, Q.; Miao, Y.; Zhang, C. Reconstructing and extracting information on SF<sub>6</sub> decomposition characteristic components induced by partial overthermal fault in GIE. *IEEE Trans. Dielectr. Electr. Insul.* **2016**, *23*, 183–193. [[CrossRef](#)]
5. Casanovas, A.M.; Casanovas, J.; Lagarde, F.; Belarbi, A. Study of the decomposition of SF<sub>6</sub> under dc negative polarity corona discharges (point-to-plane geometry): Influence of the metal constituting the plane electrode. *Evolution* **1992**, *72*, 3344–3354.

6. Beyer, C.; Jenett, H.; Klockow, D. Influence of reactive SF<sub>x</sub> gases on electrode surfaces after electrical discharges under SF<sub>6</sub> atmosphere. *IEEE Trans. Dielectr. Electr. Insul.* **2000**, *7*, 234–240. [[CrossRef](#)]
7. Zhang, X.; Dai, Z.; Wei, L.; Liang, N.; Wu, X. Theoretical calculation of the gas-sensing properties of Pt-decorated carbon nanotubes. *Sensors* **2013**, *13*, 15159–15171. [[CrossRef](#)] [[PubMed](#)]
8. Zhang, X.; Gui, Y.; Dai, Z. A simulation of Pd-doped SWCNTs used to detect SF<sub>6</sub>, decomposition components under partial discharge. *Appl. Surf. Sci.* **2014**, *315*, 196–202. [[CrossRef](#)]
9. Zhang, X.; Dai, Z.; Chen, Q.; Tang, J. A DFT study of SO<sub>2</sub> and H<sub>2</sub>S gas adsorption on Au-doped single-walled carbon nanotubes. *Phys. Scr.* **2014**, *89*, 065803. [[CrossRef](#)]
10. Zhang, X.; Yang, B.; Wang, X.; Luo, C. Effect of Plasma Treatment on Multi-Walled Carbon Nanotubes for the Detection of H<sub>2</sub>S and SO<sub>2</sub>. *Sensors* **2012**, *12*, 9375–9385. [[CrossRef](#)] [[PubMed](#)]
11. Zhang, X.; Wu, X.; Yu, L.; Zhou, J. Highly sensitive and selective polyaniline thin-film sensors for detecting SF<sub>6</sub>, decomposition products at room temperature. *Synth. Met.* **2015**, *200*, 74–79. [[CrossRef](#)]
12. Zhang, X.; Yu, L.; Wu, X.; Hu, W. Experimental Sensing and Density Functional Theory Study of H<sub>2</sub>S and SOF<sub>2</sub> Adsorption on Au-Modified Graphene. *Adv. Sci.* **2015**, *2*, 612. [[CrossRef](#)] [[PubMed](#)]
13. Varghese, O.K.; Gong, D.; Paulose, M.; Ong, K.G.; Grimes, C.A. Hydrogen sensing using titania nanotubes. *Sens. Actuators B Chem.* **2003**, *93*, 338–344. [[CrossRef](#)]
14. Mor, G.K.; Varghese, O.; Paulose, M.; Mukherjee, N.; Grimes, C. Fabrication of tapered, conical-shaped titania nanotubes. *J. Mater. Res.* **2003**, *18*, 2588–2593. [[CrossRef](#)]
15. Nakamura, R.; Tomoaki, T.; Nakato, Y. Mechanism for Visible Light Responses in Anodic Photocurrents at N-Doped TiO<sub>2</sub> Film Electrodes. *J. Phys. Chem. B* **2004**, *108*, 10617–10620. [[CrossRef](#)]
16. Valentin, C.D.; Pacchioni, G.; Selloni, A.; Livraghi, S.; Giamello, E. Characterization of paramagnetic species in N-doped TiO<sub>2</sub> powders by EPR spectroscopy and DFT calculations. *J. Phys. Chem. B* **2005**, *109*, 11414. [[CrossRef](#)] [[PubMed](#)]
17. Jagadale, T.C.; Takale, S.P.; Sonawane, R.S. N-Doped TiO<sub>2</sub> Nanoparticle Based Visible Light Photocatalyst by Modified Peroxide Sol–Gel Method. *J. Phys. Chem. C* **2008**, *112*, 14595–14602. [[CrossRef](#)]
18. Zhang, J.; Wu, Y.; Xing, M.; Leghari, S.A.K.; Sajjad, S. Development of modified N doped TiO<sub>2</sub> photocatalyst with metals, nonmetals and metal oxides. *Energ. Environ. Sci.* **2010**, *3*, 715–726. [[CrossRef](#)]
19. Yang, G.; Jiang, Z.; Shi, H.; Xiao, T.; Yan, Z. Preparation of highly visible-light active N-doped TiO<sub>2</sub> photocatalyst. *J. Mater. Chem.* **2010**, *20*, 5301–5309. [[CrossRef](#)]
20. Ho, W.; Yu, J.C.; Lee, S. Synthesis of hierarchical nanoporous F-doped TiO<sub>2</sub> spheres with visible light photocatalytic activity. *Chem. Commun.* **2006**, *111*, 1115–1117. [[CrossRef](#)] [[PubMed](#)]
21. Yu, C.; Fan, Q.; Xie, Y.; Chen, J.; Shu, Q.; Yu, J.C. Sonochemical fabrication of novel square-shaped F doped TiO<sub>2</sub> nanocrystals with enhanced performance in photocatalytic degradation of phenol. *J. Hazard. Mater.* **2012**, *237–238*, 38–45. [[CrossRef](#)] [[PubMed](#)]
22. Huang, D.G.; Liao, S.J.; Dang, Z. Preparation, characterization and photocatalytic performance of anatase F doped TiO<sub>2</sub> sol. *Acta Chim. Sin.* **2006**, *64*, 1805–1811.
23. Guo, M.; Zhang, X.; Liang, C.; Jia, G. Mechanism of Visible Photoactivity of F-Doped TiO<sub>2</sub>. *Chin. Phys. Lett.* **2010**, *27*, 204–207.
24. Li, D.; Haneda, H.; Labhsetwar, N.K.; Hishita, S.; Ohashi, N. Visible-light-driven photocatalysis on fluorine-doped TiO<sub>2</sub>, powders by the creation of surface oxygen vacancies. *Chem. Phys. Lett.* **2005**, *401*, 579–584. [[CrossRef](#)]
25. Hattori, A.; Tada, H. High Photocatalytic Activity of F-Doped TiO<sub>2</sub> Film on Glass. *J. Sol-Gel Sci. Technol.* **2001**, *22*, 47–52. [[CrossRef](#)]
26. Hazra, S.K.; Kim, N.K.; Park, J.; Choi, B.; Lee, S. Gettering by cf<sub>4</sub>-ar plasma-treated titanium within anodically bonded glass-silicon microcavities. *Sens. Mater.* **2009**, *21*, 37–51.
27. Perdew, J.P.; Wang, Y. Accurate and simple analytic representation of the electron-gas correlation energy. *Phys. Rev. B* **1992**, *45*, 13244. [[CrossRef](#)]
28. Li, D.; Ohashi, N.; Hishita, S.; Kolodiazhnyi, T.; Haneda, H. Origin of visible-light-driven photocatalysis: A comparative study on N/F-doped and N-F-codoped TiO<sub>2</sub> powders by means of experimental characterizations and theoretical calculations. *J. Solid State Chem.* **2005**, *178*, 3293–3302. [[CrossRef](#)]
29. Li, D.; Haneda, H.; Hishita, S.; Ohashi, N.; Labhsetwar, N.K. Fluorine-doped TiO<sub>2</sub>, powders prepared by spray pyrolysis and their improved photocatalytic activity for decomposition of gas-phase acetaldehyde. *J. Fluorine Chem.* **2005**, *126*, 69–77. [[CrossRef](#)]

30. Zhang, X.; Chen, Q.; Hu, W.; Zhang, J. A DFT study of SF<sub>6</sub> decomposed gas adsorption on an anatase (1 0 1) surface. *Appl. Surf. Sci.* **2013**, *286*, 47–53. [[CrossRef](#)]
31. Dong, X.; Zhang, X.; Cui, H.; Zhang, J. A first principle simulation of competitive adsorption of SF<sub>6</sub> decomposition components on nitrogen-doped anatase TiO<sub>2</sub> (101) surface. *Appl. Surf. Sci.* **2017**, *422*, 331–338. [[CrossRef](#)]



© 2017 by the authors. Licensee MDPI, Basel, Switzerland. This article is an open access article distributed under the terms and conditions of the Creative Commons Attribution (CC BY) license (<http://creativecommons.org/licenses/by/4.0/>).